

Bose-Einstein Condensates in a 1D Optical Lattice

S. BURGER, F. S. CATALIOTTI, F. FERLAINO, C. FORT, P. MADDALONI, F. MINARDI,
and M. INGUSCIO

*Laboratorio Europeo di Spettroscopia Nonlineare (LENS),
Istituto Nazionale per la Fisica della Materia (INFN),
Dipartimento di Fisica dell'Università di Firenze
Largo Enrico Fermi, 2
50125 Firenze, Italia*

Summary. — In this lecture we give an overview on current experiments on Bose-Einstein condensation (BEC) in a one-dimensional (1D) optical lattice. We introduce measurements of ground state, tunnelling and dynamical properties as well as investigations of atom optical applications and thermodynamical properties. Measurements of the coherent atomic current in an array of Josephson junctions and the critical velocity for the breakdown of superfluid motion are discussed in detail.

PACS 03.75.Fi, 03.67.Lx, 32.80.Pj – .

1. – Introduction

Bose-Einstein condensates (BECs) are quantum systems which can be easily manipulated and characterized due to their macroscopic nature [1]. The employment of BECs in atomic physics has stimulated a wealth of new experiments which is often compared to the rapid development in optics and spectroscopy after the invention of the laser [2].

Atomic BECs confined to optical lattices have been proposed for the realization of

quantum computing schemes [3, 4]. These approaches are of special interest because of the precise manipulation tools available in atomic physics.

Atoms confined in a periodic potential exhibit quantum effects known from solid state physics, like Bloch oscillations and Wannier-Stark ladders, which have been observed by exposing cold atoms to the dipole potential of far detuned optical lattices [5, 6]. The achievement of BEC has given the possibility to explore also macroscopic quantum effects in this context.

In a first experiment with BECs loaded into a 1D optical lattice, quantum interference could be observed, leading to the formation of the first “mode-locked” atom laser [7]. The coherent nature of a BEC governs its dynamics in optical lattices. From the well defined phase of the macroscopically occupied wavefunction describing the BEC it follows that at low fluid velocities the BEC is performing a superfluid motion in the lattice [8]. In a regime of a greater potential height of the optical lattice, the system is also ideally suited to study the Josephson effect: At a potential depth of the lattice sites exceeding the thermal energy BECs collectively tunnel from one site to the next, at a rate which depends on the difference in phase between the sites. Under the same conditions, thermal clouds of atoms are fixed to the wells of the optical lattice [9].

Moreover, atoms confined to tightly confining potential wells offer a controllable way to investigate ground state properties of the system [10] and lower dimensional physics, e. g., the condensation process in in lower dimensions [11].

Recently, also the squeezing of matter waves [12] and the decoherence of BECs in 2D optical lattices [13] have been investigated. Experiments, in which optical lattices are applied to the BEC on much shorter time scales have investigated Bragg-diffraction as a tool for interferometry and spectroscopy [14, 15], Bloch oscillations [16], and dynamical tunnelling [17].

Here we discuss recent experiments on macroscopic quantum effects of BEC dynamics in optical lattices. The lecture is organized as follows: In the chapter **2** we briefly introduce the setup for the implementation of an optical lattice into a BEC experiment. Chapter **3** concentrates on the Bose-Einstein phase transition in the periodically modulated trap and discusses effects of two-dimensional (2D) physics. Ground state properties of the coherent array of BECs in the optical lattice are reviewed in chapter **4**. In chapter **5** we discuss on the superfluid motion and the density-dependent breakdown of superfluidity of a BEC in an optical lattice. Chapter **6** concentrates on the direct observation of a coherent atomic current in an array of Josephson junctions. Chapter **7** concludes the paper with an outlook on future directions.

2. – Experimental setup

Techniques for the achievement of BEC in dilute atomic gases have been described in detail in Ref. [1]. In the experiments discussed in the following chapters we create BECs of ^{87}Rb by the combination of laser cooling in a double magneto-optical trap system and evaporative cooling in a static magnetic trap of the Ioffe-type [18]. The BECs are produced in the ($F=1, m_F=-1$) state, with atom numbers of the order of $N \sim 10^6$.

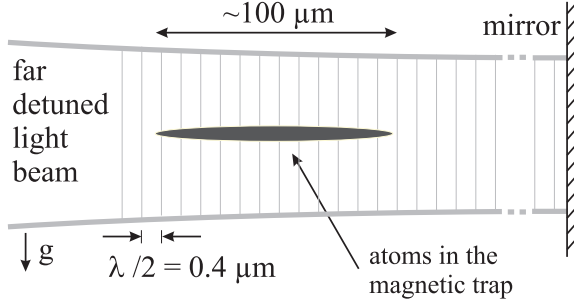


Fig. 1. – Schematic set-up of the experiment.

Due to the anisotropic magnetic trapping potential, the condensates are cigar-shaped with the long axis oriented horizontally; the typical dimensions (Thomas-Fermi radii) are $R_x \sim 60 \mu\text{m}$ and $R_\perp \sim 6 \mu\text{m}$.

We create a 1D optical lattice by superimposing to the long axis of the magnetic trap a far detuned, retroreflected laser beam with wavelength λ (see Fig. 1). The resulting potential is given by the sum of the magnetic (V_B) and the optical potential (V_{opt}):

$$(1) \quad V = V_B + V_{opt} = \frac{1}{2}m (\omega_x^2 x^2 + \omega_\perp^2 (y^2 + z^2)) + V_0 \cos^2 kx ,$$

where m is the atomic mass, $\omega_x = 2\pi \times 9 \text{ Hz}$ and $\omega_\perp = 2\pi \times 90 \text{ Hz}$ are the axial and radial frequencies of the magnetic harmonic potential, and $k = 2\pi/\lambda$ is the modulus of the wavevector of the optical lattice. By varying the intensity of the laser beam (detuned typically $\Delta = 150 \text{ GHz}$ to the blue of the D_1 transition at $\lambda = 795 \text{ nm}$) up to $14 \text{ mW}/\text{mm}^2$

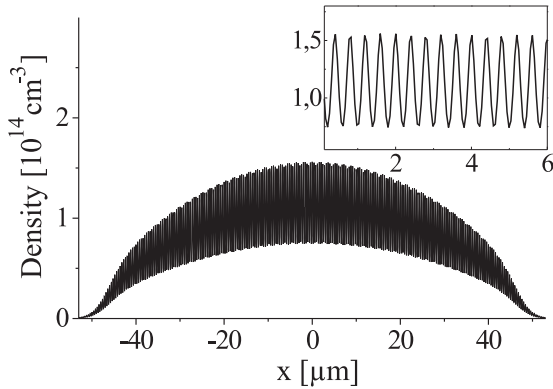


Fig. 2. – Linear density distribution of a BEC in the combined potential of the magnetic trap and optical lattice potential, obtained from a numerical simulation with the parameters $N = 3 \times 10^5$ and $V_0 = 1.5 E_R$.

we can vary the optical lattice potential height V_0 from 0 to $V_0 \sim 5E_R$, where E_R is the recoil energy corresponding to the emission or absorption of one lattice photon, $E_R = \hbar^2 k^2 / 2m$. To calibrate the optical potential we measure the Rabi frequency of the Bragg transition between the momentum states $-\hbar k$ and $+\hbar k$ induced by the standing wave [19]. Due to the large detuning of the optical lattice, spontaneous scattering can be neglected for the experiments on BEC-dynamics which are performed typically on a timescale of $\tau \sim 2\pi/\omega_x$; nevertheless, spontaneous scattering leads to a reduction of the total atom number during the preparation of the BEC.

Bose-Einstein condensates in the combined magnetic trap and optical lattice are prepared by superimposing the optical lattice to the trapping potential already during the last hundreds of ms of the RF-evaporation ramp. Figure 2 shows the expected linear density distribution of the ground state in a weakly binding lattice ($V_0 = 1.5 E_R$), as obtained by numerical propagation of the Gross-Pitaevskii equation in imaginary time. In the experiment, the density modulation on the length scale of $\lambda/2$ cannot be directly resolved, due to the limited resolution of the imaging system.

3. – Bose-Einstein phase transition lower dimensions

In this chapter we concentrate on the Bose-Einstein phase transition of the atomic gas in the combined potential of the magnetic trap and the optical lattice which allows to identify consequences of the reduced dimensionality of the system [11].

In atomic physics, important steps towards the realization of pure 2D systems of neutral atoms have been made in different systems: Significant fractions of atomic systems could be prepared in the 2D potentials of optical lattices [20, 21] and of an evanescent wave over a glass prism [22], quasicondensates could be observed in 2D atomic hydrogen trapped on a surface covered with liquid ^4He [23], and 3D condensates of ^{23}Na with low atom numbers could be transferred to the 2D regime by an adiabatic deformation of the trapping potential [24].

By using Bose-Einstein condensates (BECs) trapped in optical lattices it has become possible to overcome major limitations of previous experiments: First, an optical lattice can confine a large array of 2D systems, which allows measurements with a much higher number of involved atoms with respect to a single confining potential. Second, the macroscopic population of a single quantum state (BEC) naturally transfers the whole system to a pure occupation of the 2D systems, which could so far not be realized with thermal atomic clouds.

The dimensionality of a gas of weakly interacting bosons has important consequences for its thermodynamical properties. While in 3D the gas undergoes the phase transition to BEC even in free space, in 2D systems BEC at finite temperatures can only exist in a confining potential [25]. For the ideal gas in a 2D harmonic trap with the fundamental frequency ω the analytical solutions for the condensation temperature, T_c , and the dependence of the condensate fraction, N_0/N (number of particles in the ground state,

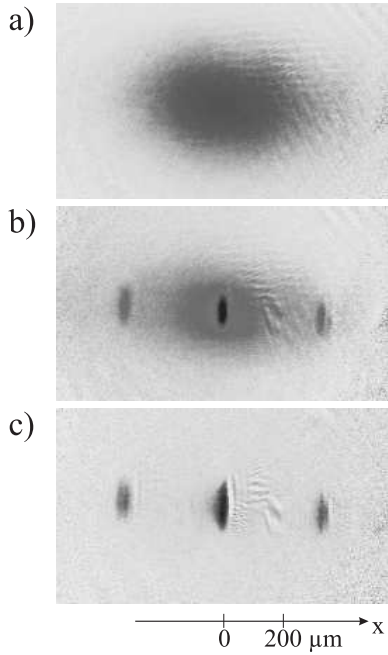


Fig. 3. – Absorption images of a thermal cloud (a), a mixed cloud (b), and a pure BEC (c), expanded for 26.5 ms from the combined magnetic trap and optical lattice ($V_0 \sim 4E_R$). The corresponding temperatures and atom numbers are $T \approx 210$ nK and $N \approx 4 \times 10^5$ (a), $T \approx 110$ nK and $N \approx 1.5 \times 10^5$ (b), $T < 50$ nK and $N \approx 1.5 \times 10^4$ (c).

N_0 , and total particle number, N) are given by [26]:

$$(2) \quad k_B T_c = \hbar\omega \left(\frac{N}{\zeta(2)} \right)^{1/2}, \quad \frac{N_0}{N} = 1 - \left(\frac{T}{T_c} \right)^2,$$

where $\zeta(s)$ is the *zeta*-function, defined as $\zeta(s) = \sum_{n=1}^{\infty} 1/n^s$. In the 3D case these dependencies are:

$$(3) \quad k_B T_c = \hbar\omega \left(\frac{N}{\zeta(3)} \right)^{1/3}, \quad \frac{N_0}{N} = 1 - \left(\frac{T}{T_c} \right)^3.$$

In our experiment, the magnetic trapping potential is a 3D potential which confines the atoms to an overall cigar-shaped distribution, while in the 1D optical lattice the atoms are confined to 2D planes. Therefore, by increasing the strength of the optical lattice superposed to a 3D potential it is possible to follow the transition from a 3D BEC to an array of 2D degenerate atomic clouds confined radially by the magnetic potential and assorted in the axial direction like disks in a shelf.

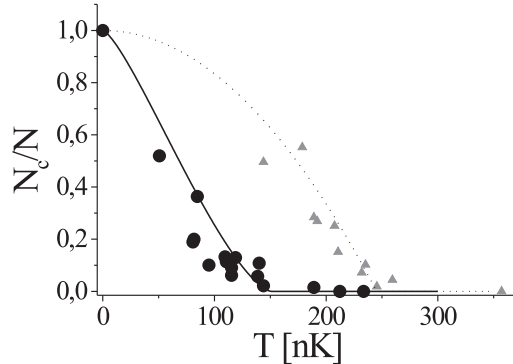


Fig. 4. – Ground state occupation vs. temperature in the combined trap with $V_0 \approx 4 E_{rec}$ (circles), and in the 3D purely magnetic trap (triangles). The solid (resp. dotted) line gives the expected dependence for the combined (resp. purely magnetic) trap, according to Eqn. 2 (resp. Eqn. 3).

For reaching the quasi 2D regime, the motion of the particles has to be effectively “frozen” in the direction of the optical lattice beam [25], i.e., the fundamental frequency in a single lattice site, ω_l has to fulfill $\hbar\omega_l \gg k_B T$. For our experimental parameters of $T < 200$ nK and $\omega_l \approx 2\pi 14$ kHz (for $V_0 \approx 4 E_{rec}$) this relation is well satisfied. Nevertheless, due to the small width of the barriers atoms can tunnel between the lattice sites. The low energy of thermal atoms allows them to tunnel only over a few sites during the duration of the experiment. Therefore we expect only minor changes of the thermodynamic properties due to such processes. In contrast, tunnelling of ground state atoms is greatly enhanced because the ground state is macroscopically occupied (see chapter 6). As a result, the BECs at the optical lattice sites form a phase coherent ensemble giving rise to the interference pattern in the expansion (see chapter 4).

In order to measure the effects of dimensionality on T_c and on $N_0/N(T)$ we have adjusted the final temperature of the atomic clouds by evaporative cooling and recorded the atomic density distributions at different temperatures. Figure 3 shows absorption images of such ensembles, expanded from a combined trap with a lattice-potential height of $V_0 \approx 4 E_{rec}$. The interference pattern of the expanding array of BECs appears in three spatially separated peaks (in Fig. 3 b,c) [10].

By integrating over the atomic density distribution we obtain the number of atoms in the ground state, N_0 , and in the thermal cloud, $N_{th} = N - N_0$. Figure 4 shows the ground state fraction N_0/N , in dependence of the temperature of the ensemble. In the case of the 3D potential of the pure magnetic trap (triangles in Fig. 4) this ratio reproduces the shape expected from Eqn. 3 (dotted line, using a linear fit to the measured function $N(T)$). The shape of the curve for ensembles produced in the combined trap is much smoother around the (lower) transition temperature and mixed clouds with a relatively

small condensate fraction exist in a broad temperature range well below T_c .

This behaviour can be qualitatively understood with a simplifying model [11] assuming the subsequent formation of 2D BECs at the different lattice sites: Due to the magnetic trapping potential the central lattice wells are populated with a higher number of atoms, which – according to Eqn. 2 – leads to a higher critical temperature for the central clouds than for the clouds in the wings of the overall density distribution. BECs form first in the central 2D disks, lowering the temperature leads to BEC formation at more and more lattice sites. The solid line in Fig. 4 shows the ground state occupation according to this model; the curve agrees well with the experimental data points. A more sophisticated theoretical modelling of the problem, including interactions and the effect of tunnelling on the thermodynamic properties, remains to be developed.

4. – Expansion of a BEC from the combined trap

In this chapter we introduce ground state properties of the fully coherent array of condensates in the optical lattice. To this aim we explore the interference pattern in the expanded cloud, reflecting the initial geometry of the sample. The time evolution of the interference peaks, their relative population as well as the radial size of the expanding cloud are compared to theoretical results developed in [10].

In analogy of multiple order interference fringes in light diffraction from a grating, the expansion of an array of coherent BECs leads for long expansion times (i.e., in the

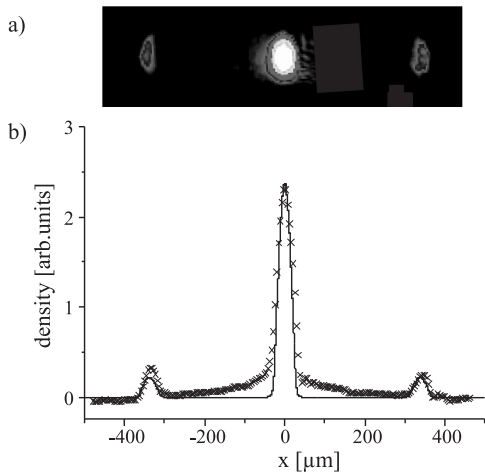


Fig. 5. – a) Absorption image of the expanded array of condensates, showing three interference peaks, $n = -1, 0, 1$. b) Density profile obtained from the absorption image (crosses) and calculated density profile for the experimental parameters $V_0 = 5E_R$ and $t_{exp} = 29.5$ ms [10]. The wings of the central peak in the experimental density profile result from a small thermal component.

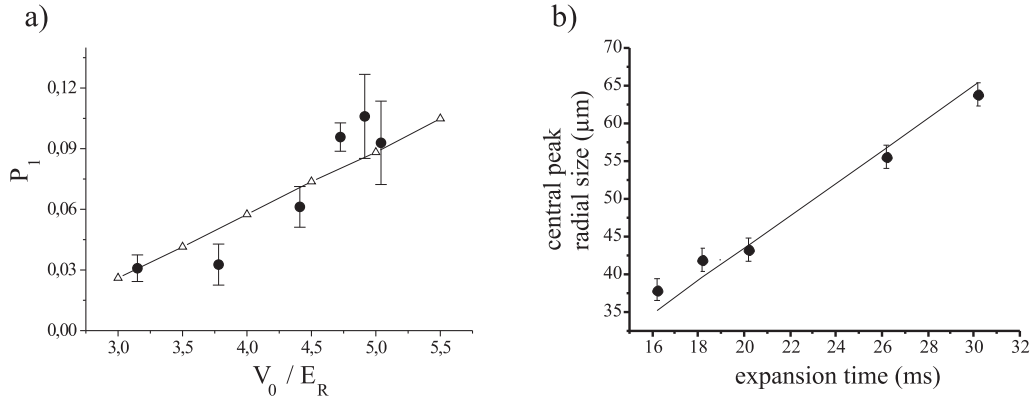


Fig. 6. – a) Experimental (circles) and theoretical values (triangles) of the relative population of the $n = 1$ peak with respect to the central one ($n = 0$) as a function of the lattice potential V_0 in units of the recoil energy E_R . b) Radial size of the central peak as a function of the expansion time. Experimental data points are compared to the expected asymptotic law $R_{\perp}(t) = R_{\perp}\omega_{\perp}t$.

far field) to distinct peaks in position space, reflecting the momentum distribution. The analogy is best understood considering a periodic and coherent array of condensates aligned along the x -axis. The momentum distribution of the whole system is affected in a profound way by the lattice structure and exhibits distinctive interference phenomena (see [10]). The momentum distribution is characterized by sharp peaks at the values $p_x = 2n\hbar k$ with n integer (positive or negative) whose weight is modulated by a function $n_0(p_x)$.

In Fig. 5a we show a typical image of the cloud taken at $t_{exp} = 29.5$ ms with a total number of atoms $N = 20000$ and a potential height of $V_0 = 5E_R$. The structure of the observed density profiles is well reproduced by the free expansion of the ideal gas assuming a periodic ground state wave function Ψ describing the array of BECs [10]. A predicted result for the density distribution $n(x) = |\Psi(x)|^2$ evaluated for the experimental parameters is shown in Fig. 5b (continuous line).

From the experimental images we determine the relative population of the lateral peak with respect to the central one. The results for the relative population of the first lateral peak as a function of the optical lattice potential V_0 are shown in Fig. 6a. This figure shows also the corresponding results of the 1D theoretical model developed in [10].

More general, it can be shown that the relative population of the $n \neq 0$ peaks with respect to the central one ($n = 0$) obeys the simple law

$$(4) \quad P_n = \exp[-4\pi^2 n^2 \sigma^2 / d^2]$$

where σ characterizes the width of a single condensate in a lattice site and d is the periodicity of the lattice, $d = \lambda/2$. Equation 4 holds also in the presence of a smooth modulation of the atomic occupation number N_k in each well. Result (4) shows that, if σ

is much smaller than d the intensity of the lateral peaks will be high, with a consequent important layered structure in the density distribution of the expanding cloud. The value of σ is determined, in first approximation, by the optical confinement. It can be obtained numerically giving $\sigma/d = 0.30, 0.27,$ and 0.25 for $V_0 = 3, 4$ and $5 E_R$ respectively [10].

A 3D model permits also to explain the behaviour of the radial expansion of the gas. In the presence of the density oscillations produced by the optical lattice the problem is not trivial and should be solved numerically by integrating the GP equation. However, after the lateral peaks are formed, the density of the central peak expands smoothly according to the asymptotic law $R_{\perp}(t) = R_{\perp}(0)\omega_{\perp}t_{exp}$, holding for a cigar configuration in the absence of the optical lattice [27]. As can be seen from Fig. 6 b the experimental values of the radial size of the peak after varied expansion time compare well to this law [10].

Concluding, we remark that the well understood behaviour of the expanding cloud can be used as a tool to investigate the coherence properties of the BEC. Deviations from the shape of the interference pattern and from the population of the interference peaks can be interpreted to result, e.g., from decoherence effects. In recent experiments, the interference peaks have been used to prove the well-defined phase relation in an array of Josephson junctions [9]. The disappearance of the interference peaks has been used to study squeezing of matter waves [12]. Further studies include the possible effects of thermal decoherence in the presence of tighter optical traps [28, 29].

5. – Superfluid dynamics

Superfluidity of BECs is a direct consequence of their coherent nature [30]. It is manifested in the appearance of vortices [31, 32] and scissors modes [33] as well as in a critical velocity for the onset of dissipative processes [34]. A far detuned optical lattice at a low potential height, $V_0 < 2 E_R$, is well suited to study in detail the critical velocity because it acts like a medium with a microscopic roughness on the BEC moving through it, being velocity-dependent compressed and decompressed as it propagates.

In order to investigate the dynamics in the combined trap we translate the magnetic trapping potential in the x -direction by a variable distance Δx ranging up to $300 \mu\text{m}$ in a time $t \ll 2\pi/\omega_x$. Therefore, the BEC finds itself out of equilibrium and is forced into motion by a potential gradient. After an evolution time t_{ev} in the displaced trap, both the magnetic trapping and the optical lattice are switched off and after a free expansion of 26.5 ms the cloud is imaged, giving information on the momentum distribution of the system.

In the magnetic trap the center-of-mass motion of the BEC in the displaced trap is an undamped oscillation with frequency $\omega_x = 2\pi \times 8.7 \text{ Hz}$ and amplitude Δx . In the combined trap formed by the magnetic and the (weakly confining, $V_0 \sim 1.5 E_R$) optical lattice potentials we observe dynamics in different regimes:

For small displacements, $\Delta x < 50 \mu\text{m}$, the dynamics of the BEC resembles the “free oscillation” at the same amplitude but with a significant shift in frequency which can be explained in terms of an effective atomic mass [8]. By varying the potential height

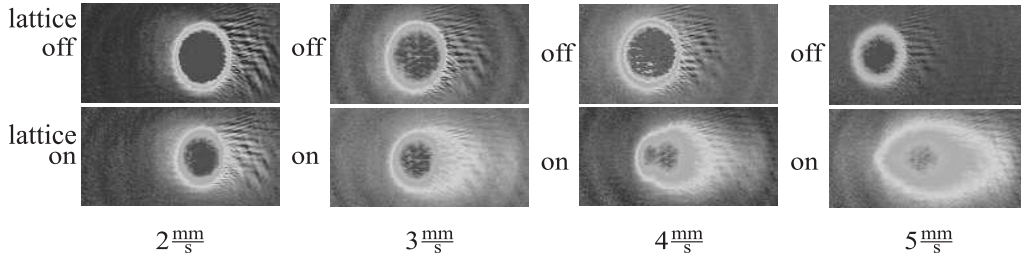


Fig. 7. – False color representation of absorption images of atomic clouds after evolution with different maximum velocities (indicated) in the magnetic trap (“lattice off”) and in the combined trap (“lattice on”).

V_0 we are able to tune this effective mass. The undamped dynamics without dissipative processes in the small-amplitude regime is a manifestation of superfluid behavior of the BEC. When we further increase the initial displacement Δx and hence the velocity of the BEC, it enters a regime of dissipative dynamics. We observe a damped oscillation in the trap and dissipative processes heating the cloud.

The critical velocity in a superfluid is proportional to the local speed of sound, c_s , which depends on the density n , $c_s(r) = \sqrt{n(r)/m (\delta\mu/\delta n)}$, with the chemical potential μ . Therefore superfluidity breaks down first in the wings of the BEC where the density is lowest.

In order to measure the velocity- and density-dependent onset of dissipation and thereby the spectrum of critical velocities in the BEC, we have varied the displacement Δx and recorded atomic distributions after a fixed evolution time $t_{ev} = 40$ ms. For low velocities, $v < 2$ mm/s, the sample follows the position of a freely moving BEC (“lattice off” in Fig. 7); no thermal component appears.

Upon increasing the velocity of the BEC, we observe a retardation of a part of the cloud, leading to a well detectable separation from the superfluid component after free evolution (see Fig. 7). For velocities $v \sim 4$ mm/s we observe that only the central part of the fluid is moving without retardation; For velocities $v \sim 4$ mm/s we observe that only a part of the fluid is moving without retardation; the central position of this part is the same as the central position of the “freely oscillating” BEC. For even higher velocities all of the atoms are retarded and form a heated cloud with a Gaussian density distribution. The spatial separation from the thermal component allows a clear demonstration of the superfluid properties of inhomogeneous Bose-Einstein condensates.

Figure 8 shows the ratio of atom number in the non-retarded component (parabolic density-profile, “superfluid component”), N_s , and the total atom number, N , in dependence of the maximum velocity attained during the evolution in the optical lattice [35]. The envelope function of the density distribution of the BEC is an inverted parabola in 3D (see Fig. 2 and hence, by integration over the high-density region, we get an equation for the relative number of atoms in the superfluid part of the BEC for a given velocity v , $N_s(v)/N = [5/2 \times (1 - v^2/v_{max}^2)^{3/2} - 3/2 \times (1 - v^2/v_{max}^2)^{5/2}]$, where v_{max}

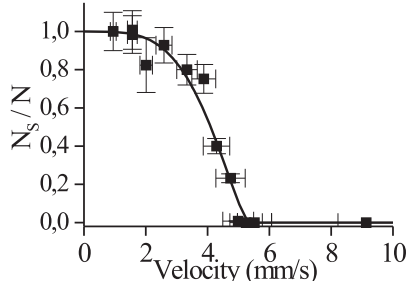


Fig. 8. – Fraction of atoms in the superfluid component vs. maximum propagation velocity.

is the critical velocity at maximum density. This expression implies that about 90% of the atomic probability density is localized in a region which remains superfluid up to velocities $v \simeq v_{max}/2$. The line in Fig. 8 shows that the above expression for $N_s(v)/N$ gives a very good account of the data, the fitted value of the maximum velocity being $v_{max} = (5.3 \pm 0.5)$ mm/s.

In the regime of a weak optical lattice potential, the lattice acts with a rather small perturbation on the BEC, the atoms are completely delocalized within the macroscopic BEC wavefunction. However, increasing the potential we reach a regime where the atoms are confined to single lattice sites. Here, the ensemble is better described in terms of an array of discrete BECs, connected to each other by tunnelling. This regime is addressed in the following chapter.

6. – Observation of a Josephson current in an array of coupled BECs

Two macroscopic quantum systems which are coupled by a weak link produce the flow of a supercurrent I between them, driven by their relative phase $\Delta\phi$,

$$(5) \quad I = I_c \sin \Delta\phi,$$

where I_c is the critical Josephson current [36, 37]. The relative phase evolves in time proportionally to the difference in chemical potential between the two quantum fluids.

The first experimental evidence of a current-phase relation was already obtained in superconducting systems soon after Josephson's proposal [38]. Also, phase-coherent tunnelling of BEC atoms from an optical lattice to the continuum, driven by gravity, has been observed [7]. We realize a one-dimensional array of bosonic Josephson junctions (JJs) by preparing an array of BECs in the sites of the optical lattice with an interwell barrier energy V_0 which is high compared to the chemical potential of the BECs [9]. Every two condensates in neighbouring wells overlap slightly with each other due to a finite tunnelling probability, and therefore constitute a JJ, with the possibility to adjust the critical current I_c by tuning the laser intensity. By driving the system with the external

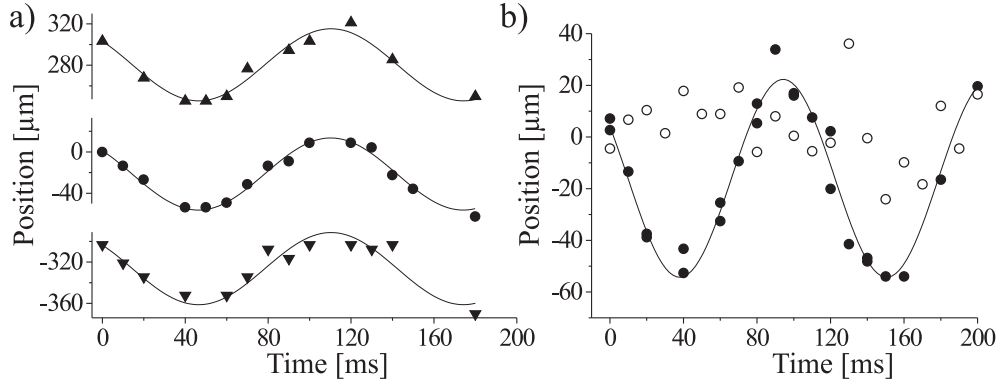


Fig. 9. – a) The three peaks of the interference pattern of an array BECs, expanded for 28 ms after the propagating in the optical lattice. b) Center-of-mass positions of thermal clouds after expansion from the magnetic trap (filled circles) and from the combined magnetic trap and optical lattice (open circles) as a function of evolution time in the displaced respective trap.

harmonic potential, we investigate the current-phase dynamics and measure the critical Josephson current as a function of the interwell potential V_0 .

In its ground state the system consists of spatially separated condensates; tunneling between adjacent wells leads to a constant phase over the whole array. Therefore, the condensates show an interference pattern after an expansion from the combined trap (see Fig. 5).

To observe a Josephson current in the array we non-adiabatically displace the magnetic trap along the lattice axis by a distance of $\sim 30 \mu m$. The potential energy the atoms gain in this process is much smaller than the interwell potential barrier, but the relative phases of the BECs in the different wells are driven by this process. According to equation 5 we expect a Josephson current. A collective motion can be established only with a well defined phase relation between the condensates. This locking of the relative

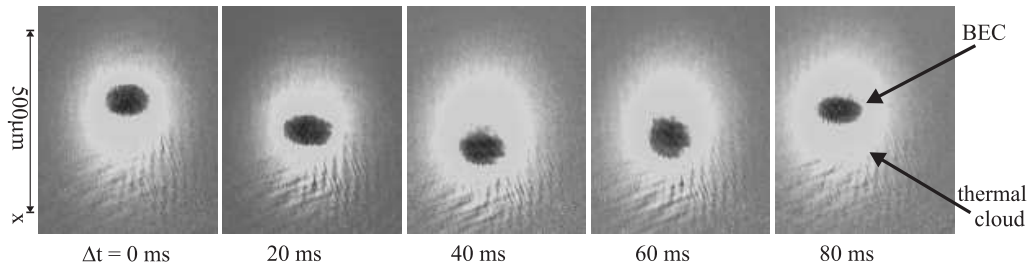


Fig. 10. – False color representation of absorption images of mixed atomic clouds in the displaced magnetic trap with superimposed optical lattice. In the time evolution Δt the ground state is moving relative to the thermal cloud.

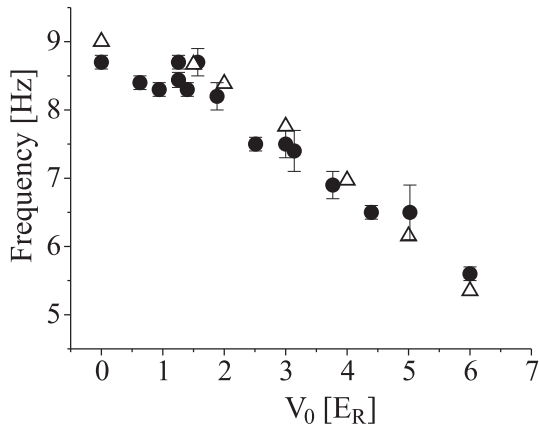


Fig. 11. – Frequency of the oscillation of a coherent ensemble in the JJ-array in dependence of the interwell potential height. Filled circles: experimental data, open triangles: results from a numerical simulation of the Gross-Pitaevskii equation [39].

phases shows up in the expanded cloud interferogram. The expected Josephson current is observed as the collective oscillation of the atomic ensemble. In Fig. 9a the positions of the three peaks in the interferogram are plotted as a function of time spent in the combined trap after the displacement of the magnetic trap. The motion performed by the center of mass of the ensemble is an undamped oscillation at a frequency $\omega < \omega_x$.

The coherent nature of the oscillation is also proven by repeating the same experiment with a thermal cloud. In this case – although atoms can individually tunnel through the barriers – no macroscopic phase is present in the cloud and no motion of the center of mass is observed. The center-of-mass positions of thermal clouds in the optical lattice are shown in Fig. 9b, together with the oscillation of thermal clouds in absence of the optical potential. As can clearly be seen, the movement of thermal clouds is strongly suppressed in presence of the optical lattice. We have also subjected mixed clouds to the displaced potential, where only the condensate fraction starts to oscillate while the thermal component remains static; the interaction of the two eventually leads to a damping of the condensate motion and a heating of the system. Figure 10 shows absorption images of mixed clouds, where a BEC moves relative to the thermal cloud.

As can be derived from the phase-current relation of the JJ array [9] the critical Josephson current is related to the small amplitude oscillation frequency ω of the JJ array by the simple relation $I_c = \frac{4\hbar}{m\lambda^2} \left(\frac{\omega}{\omega_x}\right)^2$. Figure 11 shows experimental values of the oscillation frequency ω together with results from numerical solutions of the Gross-Pitaevskii equation. The possibility to precisely adjust the critical Josephson current presents a major advantage of Josephson junctions in Bose-Einstein condensates, where due to the elaborate manipulation tools of atomic physics a variety of parameters can be

tuned, compared to systems realized in solid-state physics.

7. – Conclusions

In this lecture we have discussed thermodynamical and ground state properties of a dilute gas in the potential of an optical lattice. We have also investigated macroscopic quantum effects in the dynamics of the system, such as superfluid motion, a density-dependent critical velocity for the onset of dissipation, and – in a regime of higher lattice potentials – an oscillating Josephson current.

Future directions of this work include the study of BECs in 2D and 3D optical lattices and in superlattices, which offers the possibility of a better control of the atom number per lattice site and of the manipulation of single lattice sites, and possible applications of quantum computing schemes. We also plan to further study BEC properties in these systems, such as the dynamical behaviour of BECs in lower dimensions or the formation of bright atomic solitons in optical lattices [40].

* * *

Our understanding of the various experiments performed at LENS benefitted very much from the theoretical support in collaborations with M. L. Chiofalo, P. Pedri, L. Pitaevskii, A. Smerzi, S. Stringari, M. Tosi, and A. Trombettoni. We acknowledge stimulating discussions with M. Artoni, G. Ferrari, and G. V. Shlyapnikov. We also acknowledge support by the EU under contracts HPRI-CT 1999-00111 & HPRN-CT-2000-00125, by MURST through the PRIN 1999 & PRIN 2000 Initiatives, and by INFN under the contract “*Photon Matter*”.

REFERENCES

- [1] *Bose-Einstein Condensation in Atomic Gases* Eds. INGUSCIO M. *et al.*, (IOS Press, Amsterdam, 1999).
- [2] *Bose-Einstein Condensates and Atom Lasers* Eds. MARTELLUCCI S. *et al.*, (Kluwer, New York, 2000).
- [3] JAKSCH D., BRUDER C., CIRAC J. I., GARDINER C. W., and ZOLLER P., *Phys. Rev. Lett.*, **81** (1998) 3108
- [4] BRENNEN G. K., CAVES C. M., JESSEN P. S., and DEUTSCH I. H., *Phys. Rev. Lett.*, **82** (1999) 1060
- [5] DAHAN M. B., PEIK E., REICHEL J., CASTIN Y. and SALOMON C., *Phys. Rev. Lett.*, **76** (1996) 4508.
- [6] WILKINSON S. R., BHARUCHA C. F., MADISON K. W., NIU Q., and RAIZEN M. G., *Phys. Rev. Lett.*, **76** (1996) 4512.
- [7] ANDERSON B. P. and KASEVICH M. A., *Science*, **282** (1998) 1686.
- [8] BURGER S., CATALIOTTI F. S., FORT C., MINARDI F., INGUSCIO M., CHIOFALO M. L., and TOSI M., *Phys. Rev. Lett.*, **86** (2001) 4447.
- [9] CATALIOTTI F. S., BURGER S., FORT C., MADDALONI P., MINARDI F., INGUSCIO M., TROMBETTONI A., and SMERZI A., *Science*, **293** (2001) 843.

- [10] PEDRI P., PITAEVSKII L., STRINGARI S., FORT C., BURGER S., CATALIOTTI F. S., MADDALONI P., MINARDI F., and INGUSCIO M., *Phys. Rev. Lett.*, **87** (2001) 220401.
- [11] BURGER S., CATALIOTTI F. S., FORT C., MADDALONI P., MINARDI F., INGUSCIO M., e-print (2001) cond-mat/0108037.
- [12] ORZEL C., TUCHMAN A. K., FENSELAU M. L., YASUDA M., and KASEVICH M. A., *Science*, **291** (2001) 2386.
- [13] GREINER M., BLOCH I., MANDEL O., HÄNSCH T. W., and ESSLINGER T., *Phys. Rev. Lett.*, **87** (2001) 160405.
- [14] KOZUMA M., DENG L., HAGLEY E. W., WEN J., LUTWAK R., HELMERSON K., ROLSTON S. L., and PHILLIPS W. D., *Phys. Rev. Lett.*, **82** (1999) 871.
- [15] STENGER J., INOUE S., CHIKKATUR A. P., STAMPER-KURN D. M., PRITCHARD D. E., and KETTERLE W., *Phys. Rev. Lett.*, **82** (1999) 4569.
- [16] MORSCH O., MÜLLER J. H., CRISTIANI M., CIAMPINI D., and ARIMONDO E., *Phys. Rev. Lett.*, **87** (2001) 140402.
- [17] HENSINGER W. K., HÄFFNER H., BROWAEYS A., HECKENBERG N. R., HELMERSON K., MCKENZIE C., MILBURN G. J., PHILLIPS W. D., ROLSTON S. L., RUBINSZTEIN-DUNLOP H., and UPCROFT B., *Nature*, **412** (2001) 52.
- [18] FORT C., PREVEDELLI M., MINARDI F., CATALIOTTI F. S., RICCI L., TINO G. M., and INGUSCIO M., *Europhys. Lett.*, **49** (2000) 8.
- [19] PEIK E., DAHAN M. B., BOUCHOULE I., CASTIN Y., and SALOMON C., *Phys. Rev. A*, **55** (1997) 2989.
- [20] VULETIĆ V., CHIN C., KERMAN A. J., and CHU S., *Phys. Rev. Lett.*, **81** (1998) 5768.
- [21] BOUCHOULE I., MORINAGA M., PETROV D. S., and SALOMON C., e-print (2001) quant-ph/0106032.
- [22] GAUCK H., HARTL M., SCHNEBLE D., SCHNITZLER H., PFAU T., and MLYNEK J., *Phys. Rev. Lett.*, **81** (1998) 5298.
- [23] SAFONOV A. I., VASILYEV S. A., YASNIKOV I. S., LUKASHEVICH I. I., and JAAKKOLA S., *Phys. Rev. Lett.*, **81** (1998) 4545.
- [24] GÖRLITZ A., VOGELS J. M., LEANHARDT A. E., RAMAN C., GUSTAVSON T. L., ABO-SHAEER J. R., CHIKKATUR A. P., GUPTA S., INOUE S., ROSEN BAND T., and KETTERLE W., *Phys. Rev. Lett.*, **87** (2001) 130402.
- [25] PETROV D. S., HOLZMANN M., and SHLYAPNIKOV G. V., *Phys. Rev. Lett.*, **84** (2000) 2551.
- [26] BAGNATO V. and KLEPPNER D., *Phys. Rev. A*, **44** (1991) 7439.
- [27] CASTIN Y. and DUM R., *Phys. Rev. Lett.*, **77** (1996) 5315.
- [28] PITAEVSKII L. and STRINGARI S., *Phys. Rev. Lett.*, *in press* (.)
- [29] CUCCOLI A., FUBINI A., TOGNETTI V., and VAIA R., e-print (2001) cond-mat/0107387.
- [30] DALFOVO F., GIORGINI S., PITAEVSKII L. P., and STRINGARI S., *Rev. Mod. Phys.*, **71** (1999) 463.
- [31] MATTHEWS M. R., ANDERSON B. P., HALJAN P. C., HALL D. S., WIEMAN C. E., and CORNELL E. A., *Phys. Rev. Lett.*, **83** (1999) 2498.
- [32] MADISON K. W., CHEVY F., WOHLLEBEN W., and DALIBARD J., *Phys. Rev. Lett.*, **84** (2000) 806.
- [33] MARAGÓ O. M., HOPKINS S. A., ARLT J., HODBY E., HECKENBLAIKNER G., and FOOT C. J., *Phys. Rev. Lett.*, **84** (2000) 2056.
- [34] RAMAN C., KÖHL M., ONOFRIO R., DURFEE D. S., KUKLEWICZ C. E., HADZIBABIC Z., and KETTERLE W., *Phys. Rev. Lett.*, **83** (1999) 2502.
- [35] Due to spontaneous scattering during the preparation of the BEC in the combined trap the total atom number is reduced by a factor ~ 0.7 .
- [36] BARONE A. and PATERNO G., *Physics and Applications of the Josephson Effect* (Wiley, New York, 1982).

16 S. BURGER, F. S. CATALIOTTI, F. FERLAINO, C. FORT, P. MADDALONI, F. MINARDI, and M. INGUSCIO

- [37] SMERZI A., FANTONI S., GIOVANNAZZI S., and SHENOY S. R., *Phys. Rev. Lett.*, **79** (1997) 4950.
- [38] JOSEPHSON B. D., *Phys. Lett.*, **1** (1962) 251.
- [39] TROMBETTONI A., PhD-thesis, SISSA, Trieste, *in preparation*.
- [40] ZOBAY O., PÖTTING S., MEYSTRE P., and WRIGHT E. M., *Phys. Rev. A*, **59** (1999) 643.